Acta Crystallographica Section A
Foundations of Crystallography
ISSN 0108-7673

Received 1 February 2013
Accepted 8 April 2013

Application of δ recycling to electron automated diffraction tomography data from inorganic crystalline nanovolumes

Jordi Rius,[a]* Enrico Mugnaioli,[b] Oriol Vallcorba[a] and Ute Kolb[b]

[a]Institute of Materials Science of Barcelona (CSIC), Campus de la UAB, 08193-Bellaterra, Catalonia, Spain, and [b]Institute of Physical Chemistry, Johannes Gutemberg University Mainz, Welderweg 11, 55128 Mainz, Germany. Correspondence e-mail: jordi.rius@icmab.es

δ Recycling is a simple procedure for directly extracting phase information from Patterson-type functions [Rius (2012). *Acta Cryst.* A**68**, 399–400]. This new phasing method has a clear theoretical basis and was developed with ideal single-crystal X-ray diffraction data. On the other hand, introduction of the automated diffraction tomography (ADT) technique has represented a significant advance in electron diffraction data collection [Kolb *et al.* (2007). *Ultramicroscopy*, **107**, 507–513]. When combined with precession electron diffraction, it delivers quasi-kinematical intensity data even for complex inorganic compounds, so that single-crystal diffraction data of nanometric volumes are now available for structure determination by direct methods. To check the tolerance of δ recycling to missing data-collection corrections and to deviations from kinematical behaviour of ADT intensities, δ recycling has been applied to differently shaped nanocrystals of various inorganic materials. The results confirm that it can phase ADT data very efficiently. In some cases even more complete structure models than those derived from conventional direct methods and least-squares refinement have been found. During this study it has been demonstrated that the Wilson-plot scaling procedure is largely insensitive to sample thickness variations and missing absorption corrections affecting electron ADT intensities.

1. Introduction

Many natural and synthetic phases only appear as sub-micrometric crystals, too small for collecting single-crystal X-ray data even with synchrotron radiation. The most common technique for attaining structural information from these phases is powder X-ray diffraction (PXRD), which combines easy sample preparation (also under non-ambient conditions) with fast acquisition systems and sophisticated analytical methods. This simplicity follows from the reduction of the diffracted information to one dimension. Nevertheless, structure determination from PXRD suffers from various limitations which may be caused, firstly, by the sample [(i) a large enough amount of the sample must be available; (ii) the sample must be an almost pure phase; (iii) for nanocrystals, peak broadening due to the particle size reduces the effective data resolution range] and, secondly, by the crystal structure itself [(i) indexing of unit cells with long cell parameters is not always trivial; (ii) systematic overlap is present in high-symmetry space groups, especially in cubic ones; (iii) accidental overlap may be severe for low-symmetry space groups]. Finally, identification of the space group for crystalline phases affected by pseudo-symmetry can be problematic even for good PXRD data (see, for example, Birkel *et al.*, 2010; Rozhdestvenskaya *et al.*, 2010).

The main advantage of electron diffraction (ED) is the ability to collect single-crystal data from nanometric volumes. This is possible because electrons can be deflected and focused in quasi-parallel probes with a diameter of 10–30 nm and because the interaction with matter for electrons is much stronger than for X-rays, allowing a good signal-to-noise ratio even for diffraction originated by nanovolumes of crystalline material. Despite this, the use of ED data for structure determination purposes has been almost neglected for many years due to the dynamical effects that characterize electron scattering (Cowley, 1992). Dynamical effects originate from the strong interaction of electrons and the simultaneous excitation of several reflections, emphasized by the traditional way of collecting data in ED, based on the orientation of the crystal along prominent crystallographic axes. In order to use these data one is normally required to use methods able to model dynamical scattering, like multislice simulation (Jansen *et al.*, 1998) or Bloch waves (Dudka *et al.*, 2007). Recently, Palatinus *et al.* (2013) have applied the latter method to the full dynamic refinement from precession ED data of individual zones.

However, with the introduction of the new data-collection strategy called automated diffraction tomography (ADT) (Kolb *et al.*, 2007, 2008), less dynamical and more complete ED data are obtained which allow structure solution by using the simple kinematic approximation. The ADT strategy is based on ED patterns acquired around an arbitrary tilt axis (not corresponding to a specific crystallographic orientation) collected in sequential steps of 1° within the full tilt range of the microscope. Since reflections are measured off-zone, fewer reflections are simultaneously excited, which implies a reduction of multiple scattering and hence of dynamical effects. Moreover, completeness of the data set is generally higher, as those reflections not belonging to low-index zones are also collected. Finally, ADT data are normally acquired on one single crystal, so that merging of data from different crystals is normally not necessary. This simplifies and speeds data collection, making it possible to work also with beam-sensitive materials.

In principle, ADT can be implemented on any microscope (see, for example, Gorelik *et al.*, 2011; Palatinus *et al.*, 2011; Gemmi *et al.*, 2012). Until now, most of the structures determined by this strategy have been done in Mainz (Kolb *et al.*, 2011) thanks to the development of an acquisition routine that permits collecting nano electron diffraction (NED) patterns and tracking the crystal position in scanning transmission electron microscopy (STEM) mode. Using this procedure the electron dose on the sample is further reduced, enabling data collection of extremely beam-sensitive materials, like organics and metal–organic frameworks (MOFs) (Kolb *et al.*, 2010; Denysenko *et al.*, 2011; Feyand *et al.*, 2012; Gorelik *et al.*, 2012). ADT is often coupled with precession electron diffraction (PED) (Vincent & Midgley, 1994) to improve the accuracy of the integrated intensities (Mugnaioli *et al.*, 2009) and with cryo-apparatus to increase the stability of samples containing water and organic molecules (Denysenko *et al.*, 2011; Jiang *et al.*, 2011; Feyand *et al.*, 2012; Mugnaioli & Kolb, 2013). Tomographic acquisition has also been complemented in other laboratories with energy filtering (Gemmi & Oleynikov, 2013) and beam tilt (rotation electron diffraction, RED: Zhang *et al.*, 2010).

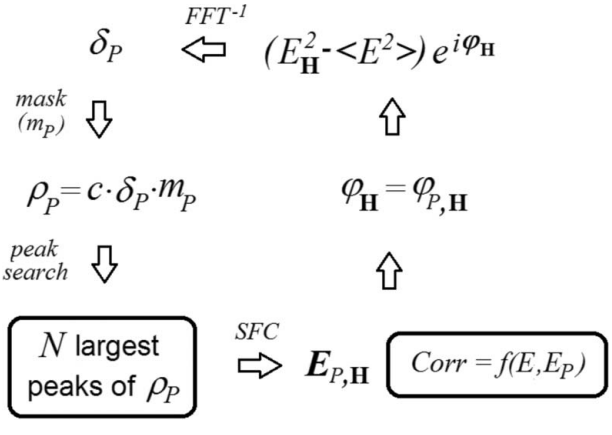

Figure 1
Schematic description of the δ_P recycling phasing procedure: starting random phase values are fed in at the upper-right corner. For ADT intensity data, the iteration stops when a preset number of cycles is reached. For the meaning of the different symbols, see the explanation in the text (*SFC* = structure-factor calculation). For δ_M recycling, $E^2 - \langle E^2 \rangle$ moduli are replaced by $E - \langle E \rangle$ and the subscripts P by M.

ADT data of inorganic compounds are not strictly kinematical as a consequence of residual dynamic effects and are also affected by experimental aspects like variable sample thickness, missing absorption correction and possible uncertainties in the intensity integration. When applying conventional direct methods, the quasi-kinematical character of the intensities can compromise the correct phasing of the reflections and result in incomplete or incorrect structural models. Recently, a simple and robust phasing procedure called δ recycling was developed and successfully tested on single-crystal X-ray diffraction data (Rius, 2012*a*,*b*). To further extend its application field, it was considered interesting to investigate the application of δ recycling to ADT data of a representative selection of inorganic compounds of variable complexity.

2. Brief description of the δ recycling procedure

2.1. The phasing stage

The δ recycling procedure is schematically described in Fig. 1. It basically consists of the minimization of the residual

$$R_{\rm P}(\Phi) = \int_V (\rho - \rho_{\rm P})^2 \, {\rm d}V \qquad (1)$$

as a function of the set $\Phi = \{\ldots, \varphi_{\mathbf{H}}, \ldots\}$ of phases of the quasi-normalized structure factors, $\boldsymbol{E}_{\mathbf{H}} = E_{\mathbf{H}} \exp(i\varphi_{\mathbf{H}})$. In $R_{\rm P}$, the density function $\rho(\mathbf{r}, \Phi)$ is compared to the modified density function

$$\rho_{\rm P}(\mathbf{r}, \Phi) = c\delta_{\rm P} m_{\rm P} \qquad (2)$$

with c being a suitable scaling constant and $\delta_{\rm P}$ being defined by the Fourier synthesis

$$\delta_{\rm P}(\mathbf{r}, \Phi) = \frac{1}{V} \sum_{\mathbf{H}} \left(E_{\mathbf{H}}{}^2 - \langle E^2 \rangle \right) \exp(i\varphi_{\mathbf{H}}) \exp(-i2\pi \mathbf{Hr}). \qquad (3)$$

The value of the $m_{\rm P}$ mask at a given $\mathbf{r}$ position in the unit cell is made zero or one depending on whether $\delta_{\rm P}(\mathbf{r})$ is smaller or larger than approximately 2.5 times its associated standard deviation, which is experimentally derivable from

$$\sigma(\delta_{\rm P}) = \left[\frac{1}{V^2} \sum_{\mathbf{H} \neq 0} \left(E_{\mathbf{H}}^2 - \langle E^2 \rangle \right)^2 \right]^{1/2}. \qquad (4)$$

The presence of the $m_{\rm P}$ mask in equation (2) ensures that $\rho_{\rm P}(\mathbf{r}, \Phi)$ is always positive. In Rius (2012*b*) it was shown that the new Φ set of phases minimizing $R_{\rm P}$ corresponds to the angular part of the Fourier transforms (structure factors) of type

$$\boldsymbol{E}_{{\rm P},\mathbf{H}} = \int_V \rho_{\rm P}\left(\mathbf{r}, \Phi^{\rm old}\right) \exp(i2\pi \mathbf{Hr}). \qquad (5)$$

As indicated in Fig. 1 with the *SFC* symbol, the $\boldsymbol{E}_{{\rm P},\mathbf{H}}$ structure factors are computed from the N largest peaks found in $\rho_{\rm P}$.

The new Φ set is then used to update δ_P. This procedure is applied cyclically until convergence is reached. Convergence is controlled by measuring the correlation between experimental E and updated E_P with the expression

$$\mathrm{Corr} = \left[\frac{\left(\sum E_{\mathbf{H}} \times E_{P,\mathbf{H}}\right)^2}{\left(\sum E_{\mathbf{H}}^2\right) \times \left(\sum E_{P,\mathbf{H}}^2\right)}\right]^{1/2}. \quad (6)$$

The Corr figure of merit clearly discriminates the correct solution when the diffraction data are accurate, *e.g.* with single-crystal X-ray data. However, our experience shows that in the case of ADT data Corr values tend to be similar for correct and wrong solutions. This is a consequence of missing corrections/perturbations that may affect the measured intensities. To circumvent this difficulty, the phasing stage always terminates when the calculation of a preset number of cycles is reached.

One peculiarity of the ADT strategy which is inherent to the data-collection geometry is the existence of an experimentally inaccessible part of the reciprocal lattice (hereafter called the missing wedge). In the case of low-symmetry compounds data incompleteness can represent a problem, especially for platelet-like crystals with prominent preferential orientation (Mugnaioli & Kolb, 2013). This is especially true when reflections along principal reciprocal-space directions are missing. In such cases the shapes of the Fourier peaks are substantially altered, so that the calculation of the Fourier transforms [equation (5)] without previous analysis of the ρ_P peaks is not recommended. Instead, it is better to refine the positions of the peak centres and to perform the posterior structure-factor calculation directly from the refined peak positions. In other words, full use of atomicity should be made (at least for the ordered parts of the crystal structure). Of course, the definitive but more time-consuming solution of the missing-wedge limitation is to fill the wedge by collecting an additional data set on cross sections through the samples, but this introduces important experimental complications in specimen preparation.

Besides the origin-free Patterson function, the origin-free modulus function can also be explored by δ recycling. The only difference between both cases is the replacement of the respective Fourier coefficients in equations (3) and (4), *i.e.* $(E^2 - \langle E^2\rangle)$ by $(E - \langle E\rangle)$. To specify the type of function used for δ recycling, the subscript P or M is added. In practice, it has been found that δ_P and δ_M behave similarly. Consequently, in the test examples both will be used.

Although the collected intensities are averaged according to the true space-group symmetry of the compound, application of δ recycling is normally performed in $P1$ symmetry (*i.e.* averaged intensities are expanded to cover one reciprocal-space hemisphere with eventual systematic absences included). Consequently, before beginning the Fourier refinement in the true symmetry, the density function solution obtained from δ recycling is first shifted to a permitted origin of the space group. This provides the centric deviation parameter,

$$\mathrm{Cendev}\ (^\circ) = \frac{180}{\pi} \times \sin^{-1}\left[\frac{\sum_{\mathbf{H}} E_{\mathbf{H}} \left|\sin\left(\varphi_{\mathbf{H}} - \varphi_{\mathbf{H},\mathrm{restricted}}\right)\right|}{\sum_{\mathbf{H}} E_{\mathbf{H}}}\right], \quad (7)$$

a useful figure of merit measuring the departure of the phase values of the centric reflections from the corresponding nearer restricted values. Only for centrosymmetrical space groups are the shifted phase values made equal to the nearest permitted values, *i.e.* 0 or 180°.

The subsequent refinement and completion of the structure model is carried out by conventional Fourier recycling methods. For non-centrosymmetric structures, the weighted $2F_o - F_c$ synthesis is used, whereas for centrosymmetric ones the weighted F_o synthesis is preferred. According to Main (1979) these syntheses approach most closely the true density function. Convergence during Fourier recycling is followed by the R_{CC} residual defined by

$$R_{CC} = 1000 \times \left\{1 - \frac{\left[\sum (F_{\mathbf{H}} F_{c,\mathbf{H}})^{1/2}\right]^2}{\sum F_{\mathbf{H}} \sum F_{c,\mathbf{H}}}\right\}, \quad (8)$$

which is free from scaling factors. For X-rays, R_{CC} is always a very reliable figure of merit and values between 5 and 30 indicate correct solutions; for ADT data, essentially correct solutions are between 15 and 60, although R_{CC} values up to 80 can be reached, especially if the data are affected by large thickness variations and/or by residual dynamic scattering, if missing organic parts of the structure are not included in the calculation of the intensities, or if the measured data fail to produce well shaped peaks in the Fourier map.

2.2. The scaling of ADT intensities

In single-crystal X-ray experiments the whole crystal is embedded in the beam to keep the illuminated sample volume constant. However, when applying the ADT technique to non-spherical samples in the NED mode, the illuminated nano-volume varies with the sample orientation. The illuminated portion is defined by the cross-sectional area S of the primary electron beam and by the sample thickness t along the direction of the primary beam. Since the ADT technique measures the data at different sample orientations and since S is constant, the sample thickness will be a function of the sample orientation. One example is provided by a platelet having the tilt-axis direction included in the platelet plane. In this case, t values gradually change with the tilt angle (large dispersion of t values).

According to Vainshtein (1991), a criterion for evaluating the applicability of the kinematical theory to a nanocrystal is that $\lambda[F(\mathbf{H})/V]t \leq 1$ where $F(\mathbf{H})$ are the structure amplitudes for electrons and λ is the wavelength of fast electrons. The critical value of t for crystals only containing medium and light atoms is about 20–40 nm. As t surpasses the critical value, the probability increases that multiple scattering occurs. Fortunately, the combination of the ADT collection strategy with the PED technique reduces the incidence of dynamical diffraction. If I_o is the intensity of the incident beam and k is a suitable constant scaling factor for a given crystal, the

dependence of the integrated intensity $I(\mathbf{H})$ on the squared structure-factor amplitude may be expressed for an arbitrary $\mathbf{H}$ reflection in the form

$$I(\mathbf{H})/p(\mathbf{H}) = kI_oSg(\mathbf{H})F(\mathbf{H})^2, \tag{9}$$

where $g(\mathbf{H})$ is a general term expressing the overall diminution of the intensity with thickness and $p(\mathbf{H})$ is a waste-bin correction for whatever remains after the best possible correction for thickness. For a fixed tilt axis, $g(\mathbf{H})$ can be written in the form

$$g(\mathbf{H}) = \langle g\rangle\alpha(\mathbf{H}), \tag{10}$$

where g is averaged over all $\mathbf{H}$ reflections. $\alpha(\mathbf{H})$ measures the deviation of $g(\mathbf{H})$ from $\langle g\rangle$ and, according to its definition, its average, $\langle\alpha\rangle$, must be one. Similarly, $p(\mathbf{H})$ may be decomposed into the product

$$p(\mathbf{H}) = \langle p\rangle\eta(\mathbf{H}), \tag{11}$$

where the average is taken again over all $\mathbf{H}$ reflections with $\langle\eta\rangle = 1$. Finally, by defining the new constant,

$$c' = kI_oS\langle p\rangle, \tag{12}$$

equation (9) reduces to

$$I(\mathbf{H})/\eta(\mathbf{H}) = c'F(\mathbf{H})^2g(\mathbf{H}). \tag{13}$$

The Wilson plot requires the reciprocal space to be divided into $N_{\rm shell}$ concentric spherical shells, each one including enough reflections to give a representative average (j = 1 to $N_{\rm shell}$). If $\mathbf{H}(j)$ are the reflections in an arbitrary j shell, the average of equation (13) for this shell is

$$\langle I(\mathbf{H})/\eta(\mathbf{H})\rangle_{\mathbf{H}(j)} = c'\langle g(\mathbf{H})F(\mathbf{H})^2\rangle_{\mathbf{H}(j)}, \tag{14}$$

which, in view of the fact that $g(\mathbf{H})$ and $F(\mathbf{H})^2$ are uncorrelated quantities, can be simplified to

$$\langle I(\mathbf{H})/\eta(\mathbf{H})\rangle_{\mathbf{H}(j)} = c'\langle g\rangle_{\mathbf{H}(j)}\langle F(\mathbf{H})^2\rangle_{\mathbf{H}(j)}. \tag{15}$$

For ADT and for fast electrons (very small Bragg angle), all nodes close to a reciprocal-space plane specified by a given tilt axis and tilt angle and passing though the origin will diffract almost simultaneously. By assuming a slow dependence of g with the tilt angle, it may be assumed that all these nodes will have similar g values. Consequently (within the limits imposed by this approximation), the average g values of the individual shells involved in the Wilson plot can be considered equal. This means that each $\langle g\rangle_{\mathbf{H}(j)}$ can be replaced by a constant $\langle g\rangle$ in equation (15), thus giving

$$\langle I(\mathbf{H})/\eta(\mathbf{H})\rangle_{\mathbf{H}(j)} = c'\langle g\rangle\langle F(\mathbf{H})^2\rangle_{\mathbf{H}(j)}, \tag{16}$$

which is valid for any j shell. If the kinematical theory applies (as is supposed in the present study), then $\eta(\mathbf{H})$ will be close to one for all $\mathbf{H}$, and therefore $N_{\rm shell}$ equalities of the type in equation (16) will be available for the calculation of the Wilson plot (Wilson, 1942).

To estimate the errors associated with the Wilson-plot scaling procedure, the $R_{\rm Wilson}$ residual is introduced which is defined by

$$R_{\rm Wilson} = 1000 \times \left[1 - N_{\rm shell}^{-1}\left(\sum_j Q_j\right)^2 \Big/ \sum_j Q_j^2\right] \tag{17}$$

with

$$Q_j = \langle I(\mathbf{H})\rangle_{\mathbf{H}(j)}/\langle F_{\rm c}(\mathbf{H})^2\rangle_{\mathbf{H}(j)}, \tag{18}$$

i.e. the discrepancies of each Q_j from unity are measured. From our experience $R_{\rm Wilson}$ values below 40 can be considered normal for ADT data of inorganic compounds.

2.3. Influence of intensity uncertainties on δ recycling

δ Recycling is based on the convolution of the origin-free Patterson function P′ with the phase synthesis. In the X-ray case, there is no problem to compute P′ accurately since the $E(\mathbf{H})^2 - \langle E^2\rangle$ coefficients are known. For electrons, the relationship between the experimental intensities and the quasi-normalized amplitudes can be found by dividing both sides of equation (13) by

$$K(\mathbf{H}) = c'\langle g\rangle \exp[-2B_{\rm over}(\sin^2\theta_{\mathbf{H}}/\lambda^2)]\sum_j^N f_{o,j}(\theta_{\mathbf{H}})^2, \tag{19}$$

with $f_{o,j}$ being the stationary electron scattering factor for atom j and with c' and $B_{\rm over}$ being, respectively, the scaling factor and the overall atomic displacement parameter derived from the Wilson plot. This gives the normalized intensity

$$I_n(\mathbf{H}) = I(\mathbf{H})/K(\mathbf{H}) = \eta(\mathbf{H})\alpha(\mathbf{H})E(\mathbf{H})^2 \tag{20}$$

since, because of equation (10), $\alpha(\mathbf{H}) = g(\mathbf{H})/\langle g\rangle$. A Fourier synthesis with the experimental $I_n(\mathbf{H})$ as Fourier coefficients yields the $P_{\rm exp}$ Patterson function with its value at the origin being

$$P_{\rm exp}(0) = \frac{N_{\rm ref}}{V}\langle I_n(\mathbf{H})\rangle_{\mathbf{H}}. \tag{21}$$

In view of equation (20) and assuming for simplicity an equal-atom structure, $I_n(\mathbf{H})$ can be expanded in terms of the interatomic vectors, $\mathbf{r}_j - \mathbf{r}_k = \mathbf{r}_{jk}$, according to

$$I_n(\mathbf{H}) = \eta(\mathbf{H})\alpha(\mathbf{H}) + \frac{1}{N}\sum_j^N\sum_{k\neq j}^N \eta(\mathbf{H})\alpha(\mathbf{H})\exp(-i2\pi\mathbf{H}\mathbf{r}_{jk}). \tag{22}$$

By incorporating this expansion into the Patterson synthesis expression, it follows that $P_{\rm exp}(0)$ is equal to $(N_{\rm ref}/V)\langle\eta(\mathbf{H})\alpha(\mathbf{H})\rangle_{\mathbf{H}}$, which can be estimated from equation (21). Consequently, the Patterson synthesis with coefficients $I_n(\mathbf{H}) - \langle I_n\rangle$ corresponds to $P_{\rm exp}$ with removed origin peak, *i.e.*

$$P'_{\rm exp}(\mathbf{u}) = \frac{N_{\rm ref}}{NV}\sum_j^N\sum_{k\neq j}^N\langle\eta(\mathbf{H})\alpha(\mathbf{H})\exp[-i2\pi\mathbf{H}(\mathbf{u} - \mathbf{r}_{jk})]\rangle_{\mathbf{H}}. \tag{23}$$

$P'_{\rm exp}(\mathbf{u})$ only contains the contributions of the interatomic vectors, $\mathbf{r}_j - \mathbf{r}_k = \mathbf{r}_{jk}$ (with $k \neq j$), and represents the best approximation to P′ that can be obtained from the ED experiment. Compared to P′, the presence in equation (23) of $\eta(\mathbf{H})\alpha(\mathbf{H})$ products different from one introduces some noise

Table 1
Crystal data of the selected test compounds with estimated errors of 2–3% on cell parameters and 0.5° on angles.

Code	Space group	Formula	Z	a (Å)	b (Å)	c (Å)	α (°)	β (°)	γ (°)
S124	*Pnma*	$Sr_2P_6N_{10}O_2$	8	18.33	8.09	13.85	90	90	90
ZSM-5	*Pnma*	$(Al,Si)_{12}O_{24}Na$	8	20.10	19.92	13.42	90	90	90
CHA90	$P2_1/m$	$K_4(Ca,Na)_8Si_{17.5}(O,OH)_{184}$	4	31.96	19.64	7.09	90	~90	90
ITQ-43†	*C*222	$Si_{12.3}Ge_{6.7}O_{40}$	8	26.09	41.87	12.84	90	90	90
IM-5	*Cmcm*	$Si_{18}O_{36}$	16	14.21	57.24	19.99	90	90	90
AER	*P*3*c*1	$Ca_{5.4}Fe_2^{3+}Fe_{1.3}^{2.5+}Al_{6.7}Si_{12}O_{36}(OH)_{16.1}(H_2O)_{1.3}$‡	1	16.88	16.88	5.23	90	90	120

† Only the framework is considered. ‡ Approximate composition disregarding minor constituents like Mg, CO_3^{2-}, SO_4^{2-}.

in P'_{exp} except for $\mathbf{u} = \mathbf{r}_{jk}$. At these particular points the values of all exponential terms are one, which implies that the function P'_{exp} is peaked with strength at the maximum given by

$$P'_{exp}(\mathbf{r}_{jk}) = \frac{N_{ref}}{NV}\langle\eta(\mathbf{H})\alpha(\mathbf{H})\rangle_{\mathbf{H}}, \quad (24)$$

i.e. the strengths are constant and identical for all peaks at $\mathbf{u} = \mathbf{r}_{jk}$. Since $\langle\eta(\mathbf{H})\alpha(\mathbf{H})\rangle$ cannot be too far from one, P' and P'_{exp} must practically coincide at the peak maxima. Strictly speaking, this coincidence is only valid for a Patterson function having all interatomic peaks well resolved. If this is the case, then both the positions and the relative strengths of the N highest peaks in function $\delta_P m_P$ (which is the convolution of P' with the phase synthesis followed by the mask application) will be accurate (provided, of course, that the phase synthesis is correctly phased). In other words, the $E_P(\mathbf{H})$ structure factors [equation (5)] calculated from the positions and heights of these N peaks are rather insensitive to the presence of (moderate) intensity uncertainties. In the case of inorganic compounds the peaks in the Patterson function tend to be well separated owing to the long interatomic distances (compared, for example, to organic compounds), which explains the accurate results from δ recycling. The use of high-resolution data also helps to diminish peak overlap, since then Patterson peaks are sharper.

The figure of merit computed during δ recycling is the Corr correlation coefficient. Although its definition [equation (6)] is given in terms of E values, in practice, $(I_n)^{1/2}$ are the observed data being correlated with the corresponding E_P calculated from the atomic peaks located in the previous refinement cycle. Two obvious conditions which are necessary for reaching high Corr values are: (i) that the estimated E_P are correct and (ii) that the observed $(I_n)^{1/2}$ values are accurate enough, *i.e.* that most $\alpha(\mathbf{H})\eta(\mathbf{H})$ products are not too far from one. Closely related to Corr is the R_{CC} residual [equation (8)]. Since a correlation coefficient is also involved in its definition, similar arguments are valid for Corr and R_{CC}. The main difference between the two figures of merit is in the correlated quantities, which are $I^{1/2}$ and F for the latter. R_{CC} is calculated at the end of the conventional Fourier refinement and, since it involves further refined phases than Corr, it is in general more informative.

3. General aspects of ADT data collection

ADT measurements were carried out with an FEI Tecnai F30 S-TWIN transmission electron microscope working at 300 kV. NED patterns were acquired with a CCD camera (14-bit Gatan 794MSC). STEM images for crystal tracking during the tilt were acquired by a Fischione high angular annular dark field (HAADF) detector. For ADT acquisition samples were mounted on a Fischione tomography holder and on a Gatan cryo single-tilt holder.

In order to perform ADT acquisition with a mild illumination on the sample, the automatic routine described in Kolb *et al.* (2007) was used. ED patterns were acquired in NED mode and after each tilt step the position of the crystal was tracked by STEM. A condenser aperture of 10 µm and mild illumination conditions (gun lens 8, spot size 6 or 8) were used in order to produce a quasi-parallel beam of 50 to 100 nm in diameter on the sample and to reduce the electron dose. In certain cases just a corner or an edge of a micrometric crystal was measured. The only condition is that the number of unit cells in the illuminated volume must be large enough to ensure that the diffracted intensities form sharp maxima at the reciprocal-lattice nodes. PED was performed with a NanoMEGAS Digistar unit. The precession angle was kept at 1.2°. Self-developed software packages and the *ADT3D* package (NanoMEGAS, Belgium) were used for data processing, including three-dimensional diffraction volume reconstruction and inspection, cell vector determination and intensity integration. No correction for the Lorentz factor was applied to PED intensities.

4. Applications of δ recycling to ADT data of selected inorganic compounds

Some important aspects of the application of δ recycling to ADT data are analysed with the help of the test structures given in Table 1. Of the three zeolites tested (codes ZSM-5, IM-5 and ITQ-43), the first two are in calcined form while the third one is 'as synthesized', *i.e.* still including the template molecules. The codes AER and CHA90 refer to the aerinite and charoite90 silicate minerals. Finally, the oxonitridophosphate S124 has been included to show some present limitations of ADT data for crystal structures with partial occupancies. Relevant experimental information about the various ADT data sets is summarized in Table 2. The $R_{sig}(F)$ =

Table 2
Detailed experimental information for the test examples.

d_{min}, minimum d spacing (Å) for δ recycling. In the 'Tilt range' row, two values indicate that the final data set results from two merged tilt series on the same crystal (except for ITQ-43). Cov, coverage (%) of weighted reciprocal lattice down to d_{min}. N_{tot}, total number of collected intensities. N_{asi}, number of intensities of symmetry-independent reflections. $R_{sig}(F) = \sum\sigma(F)/\sum F$ includes all reflections (with more than one symmetry-related reflection) down to d_{min}. $R1(F) = \sum|F_{av} - F_c|\sum F$ where F_{av} is the value obtained from averaging the amplitudes of the symmetry-related reflections and F_c is calculated from the least-squares refined model (*SHELX97*). R_{Wilson}, residual defined in equation (19) measuring the discrepancies of each $\langle I(\mathbf{H})\rangle_{shell}/\langle F_c(\mathbf{H})^2\rangle_{shell}$ quotient from unity, for five shells. B_{over}, overall atomic displacement parameter.

	Code					
	S124	ZSM-5	CHA90	ITQ-43†	IM-5	AER
d_{min} (Å)	1.00	1.00	1.18	1.15	1.00	0.70
Tilt range (°)	120+95	120	120+95	100+100	106+102	120
Cov (%)	86.0	79.2	97.2	98.8	93.6	99.4
N_{tot}	5423	16037	8418	12838	17926	5210
N_{asi}	1083	2398	2883	2688	4355	1314
R_{sig} (%)	17.0	24.1	14.9	26.7	20.6	21.1
$R1$ (%)	25.0	28.2	17.3		26.0	21.3
R_{Wilson} (%)	10.7	8.4	10.3	101.2	37.9	30.9
B_{over} (Å^2)	4.6	4.2	3.5	2.9	1.0	2.5

† Data taken at 115 K.

$\sum\sigma(F)/\sum F$ residual measures the similarity of the amplitudes among symmetry-related reflections down to d_{min} (only those reflections with more than one symmetry-related reflection are included in the sum). In addition, to give an idea of the deviation of the data from kinematicity, the $R1(F) = \sum|F_{av} - F_c|/\sum F$ residual has been added. In $R1$, F_{av} is the value resulting from averaging the amplitudes of the symmetry-related reflections and F_c is the corresponding value calculated from the least-squares refined model (the observations, F_{av}, are assumed to be free from systematic errors). Because of the incomplete location of the template molecule, the ITQ-43 case has been excluded. Table 2 also shows the numerical results of the Wilson plots. For most test structures the B_{over} and R_{Wilson} values are reasonable. The only exception is the large R_{Wilson} value for ITQ-43 zeolite, which is surely related to the omission of the template molecules in the unit-cell contents and to the merging of two data sets coming from different crystals. The theory developed in §2.2 only applies to the ZSM-5 and AER cases, since only these data sets were collected with unique tilt axes. For AER the R_{Wilson} value at 1 Å resolution is 19.8.

δ Recycling calculations have been carried out on a PC with a slightly modified version of *XLENS_v1* which can be retrieved from http://www.icmab.es/crystallography/software subject to the conditions specified there. The atomic scattering factors for electrons used in δ recycling were derived from the atomic scattering factors for X-rays (Mott & Massey, 1965); for least-squares refinement with *SHELX97* (Sheldrick, 2008), tabulated scattering factors for electrons were used (Doyle & Turner, 1968). More information on the calculations discussed in this section can be found in the supplemetary information.[1]

4.1. S124: a difficult case of structure model completion

Oxonitridophosphates are an emerging class of materials with interesting applications owing to their ability to form different frameworks. The development of these materials is partially hindered by the difficulties in producing large crystals and pure syntheses. Recently, SrP_3N_5O (Sedlmaier *et al.*, 2011) and $Ba_6P_{12}N_{17}O_9Br_3$ (Mugnaioli *et al.*, 2012) were solved on the basis of ADT data. SrP_3N_5O forms needles and its crystal structure is particularly challenging because of the presence of 25 independent atoms, most of which are light atoms (N and O). Sedlmaier *et al.* (2011) refined the N and O distribution by placing one O atom at a definite site and the rest at many sites partially replacing N. During the least-squares refinement 60 distance restraints of the type P—(N,O) and (N,O)···(N,O) were introduced. Final figures of merit were $R1 = 0.30$, $wR2 = 0.66$, goodness-of-fit (GoF) = 2.53 for 1360 observed reflections with $F_o^2 > 2\sigma(F_o)^2$ (*SHELX97*; Sheldrick, 2008).

δ_M Recycling was checked on the same set ($d_{min} = 1$ Å) and yielded 23 correct solutions out of a total of 25 trials (68 cycles per trial; 5 s per trial). The figures of merit for the correct solutions are R_{CC} = 24–29; Corr = 0.90–0.91; Cendev = 12–15°. For the wrong solutions, R_{CC} = 71–72 and Corr = 0.88–8.87. The resulting atomic positions are shown in Fig. 2.

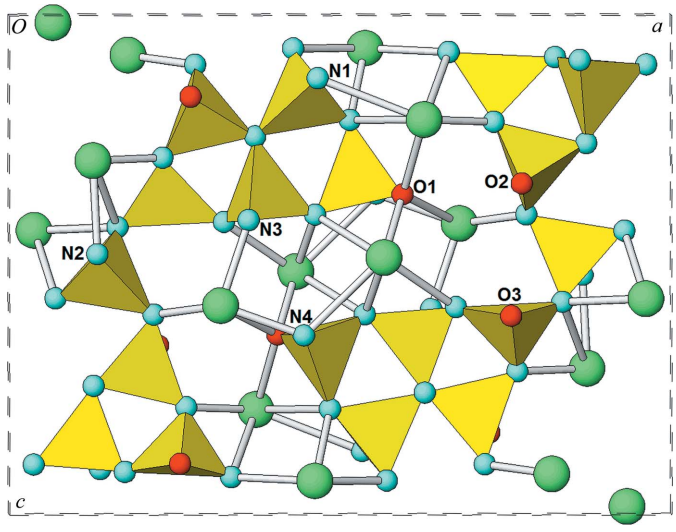

Figure 2
Perspective view of the unit cell along **b** showing the proposed structure model of S124 as obtained from ADT data by δ_M recycling and by posterior crystal chemical interpretation (only bonds between atoms inside one unit cell are represented; the maximum bond length is 3.15 Å). Large (green) circles: Sr; small circles at the vertices of the P tetrahedra are: N (light blue) and O (red). Atom O1 is linked to one P and three Sr and was already identified by Sedlmaier *et al.* (2011). The structure propagates along **b** through the bridging N1, N2, N3, N4, O2, O3 atoms lying on a mirror plane and connecting each one to two mirror-related P tetrahedra (for clarity, symmetry-related bridging N,O have not been labelled). In the proposed simpler model, the bridging atoms not bound to Sr are assumed to be O atoms (O2, O3).

[1] Supplementary material for this paper is available from the IUCr electronic archives (Reference: SC5059). Services for accessing these data are described at the back of the journal.

Owing to the similar scattering powers of N and O, it is very difficult to find their distribution in the unit cell. In addition, since atomic distances refined from ADT data are less accurate than those derived from X-ray data, the crystal chemical information that can be derived from the distances is limited. The statistical analysis of the Fourier peaks gives:

(i) The average value of the mean P—(N,O) distances of the six independent tetrahedra in the unit cell is 1.61 (5) Å [expected P—N and P—O distances are, respectively, 1.65 and 1.52 Å for a bond strength of 1.25 valence units (v.u.) (Brese & O'Keefe, 1991)]. Since the number of N to O atoms is 5 to 1, the average value, 1.614 Å, is close to the expected one.

(ii) The average value of the standard deviations corresponding to the four P—(N,O) distances in each tetrahedron is 0.10 Å (this value also incorporates the difference in P—N and P—O bond lengths).

It is clear from (ii) that the P—(N,O) distances are not very reliable. To derive a plausible model, analysis of the coordination of the ligands is preferable in this case. From the 96 existing ligands in the unit cell, 80 ligands have either a triangular or a tetrahedral coordination with two bonds to P atoms and the rest to Sr atoms, eight ligands are exclusively bound to two P atoms and the last eight have a tetrahedral coordination with one bond to a P atom and three weaker bonds to Sr atoms. By assuming that the eight bridging ligands and the eight ligands bound to only one P are O atoms, a chemically reasonable crystal model is obtained that also fulfils the known N:O ratio, *i.e.* 80:16 = 5:1. (A detailed description of the proposed model is given in Fig. 2.) The least-squares refinement of this simpler model (only including 24 restraints of the type P—N and P—O) yields lower figures of merit [$R1 = 0.25$, $wR2 = 0.60$, GoF = 2.20 for 1359 reflections with $F_o > 4\sigma(F_o)$] which seems to validate it. S124 is a particularly difficult case. Fortunately, not all structure models are so difficult to complete. However, there is no doubt that the improvement in the accuracy of bond-length estimations is an important issue that is closely related to the progress in data-acquisition techniques and data-treatment procedures.

4.2. ZSM-5: effect of the systematic omission of reflections on the peak form

ZSM-5 is one of the most important zeolites for catalytic applications. The framework topology and the structural features of ZSM-5 were first described in Kokotailo *et al.* (1978). Later, an X-ray diffraction study on a small single crystal of dehydrated ZSM-5 with an Si/Al atomic ratio equal to 94.9/1.1 followed (Olson *et al.*, 1981). ZSM-5 consists of 12 independent tetrahedral sites and typically crystallizes in a platelet-like shape, often affected by germination. As pointed out by the authors, the small size of the crystal employed in the X-ray diffraction study limits the extension of the Cu $K\alpha$ data set and, consequently, slightly increases the uncertainty of the refined atomic positions, *e.g.* ~0.06 Å for the O atoms.

An ADT data set of a ZSM-5 sample with a similar Si/Al ratio (93.9/2.1) was collected from a broken fragment with the reflections of $h00$ type missing (Mugnaioli & Kolb, 2013). From 25 δ_M trials with random initial phases, 22 developed the correct solution (150 cycles per trial; 36 s per trial). The figures of merit for the successful runs are: R_{CC} = 59–65; Corr = 0.874–0.865; Cendev = 16–19°. For the wrong solutions, R_{CC} = 95–117 and Corr = 0.867–0.846. The effect of leaving out the $h00$ reflections is seen in the clear elongation along **a** of the Fourier peaks (Fig. 3). In this specific case all bridging O atoms could be identified in most solutions by the peak-search subroutine in spite of the marked peak elongation; however, in other cases this effect can compromise the routines for automatic Fourier map interpretation.

Comparison of the positions of the framework atoms obtained for one arbitrarily selected correct δ_M solution with the corresponding positions from the single-crystal X-ray study gives an average deviation of 0.16 (7) Å for the Si atoms and of 0.22 (9) Å for the O atoms. To evaluate the significance of these deviations, the atomic positions derived from a published X-ray Rietveld refinement (Mentzen, 2007) of a ZSM-5 sample showing a similar Si/Al ratio (89.1/6.9) are also compared to the single-crystal ones. In this case the respective average deviations for the Si and O atoms are 0.14 (6) and 0.21 (10) Å, *i.e.* in the same order as the previous ones.

To complete this analysis, the average distortions of the tetrahedral coordination in the three compounds are also compared. The distortion is measured by the average O—Si—O value and its associated standard deviation. The values found are 109 (6)° for the δ_M solution, 109 (7)° for the single-crystal study and 109 (4)° for the Rietveld refinement. The fact that the Rietveld refinement data show more regular tetra-

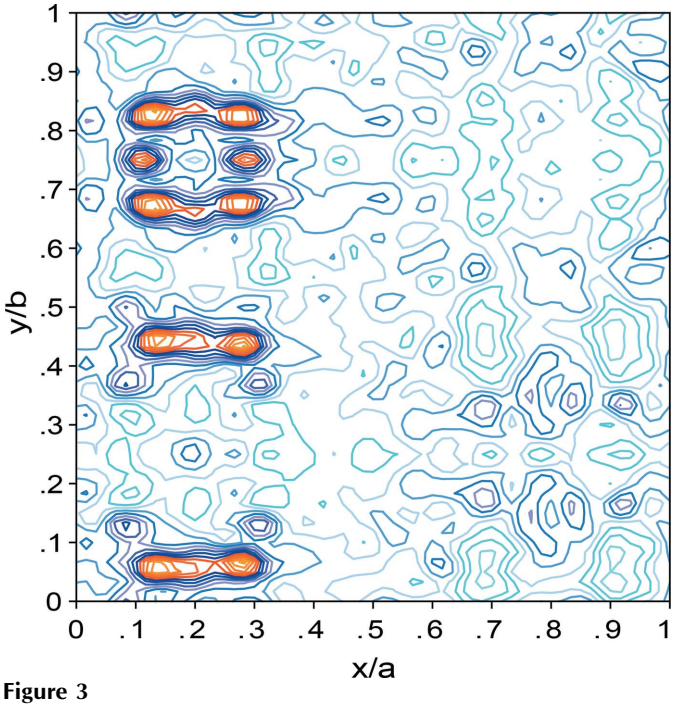

Figure 3
Section of the Fourier map through a four-membered ring of zeolite ZSM-5 (upper square) affected by peak elongation along **a** caused by the missing $h00$ reflections. From the two types of bridging O atoms present in the ring, peak-search procedures will find it difficult to locate only one type.

hedra (smaller standard deviation) may be attributed to the use of restraints.

4.3. Charoite90: effect of a large number of independent atoms on the convergence of δ recycling

Charoite is a semi-precious mineral outcropping only found in the Murun massif in Yakutiya, Russia. This mineral forms nanometric intergrown fibres aggregated with other minerals like quartz, pectolite and apophyllite. Charoite had eluded structure determination by PXRD for several decades for a number of reasons: (i) the neighbouring minerals form well developed crystals while charoite is limited to the nanometric size; consequently, the sharpest peaks in PXRD patterns do not belong to charoite, while charoite itself gives only broadened reflections. (ii) Charoite forms several commensurate polytypes related to different order–disorder sequences. There are two polytypes of maximum order: charoite90 and charoite96, differing in the monoclinic β angle. (iii) Charoite90 (CHA90), the most abundant polytype, is characterized by a strong pseudo-symmetry. While its metric is orthorhombic, its space group is monoclinic. Consequently, for determining the correct symmetry and properly integrating the reflection intensities a three-dimensional data set is compulsory. (iv) Charoite is a very complex mineral with a structure consisting of about 90 atoms in the asymmetric unit.

An outstanding electron diffraction data set for CHA90 was finally achieved merging two ADT acquisitions performed on the same crystal with orthogonal tilt axes (TILT_1 and TILT_2) (Rozhdestvenskaya *et al.*, 2010). The reason for merging two data sets was the impossibility of solving the structure by applying conventional direct methods to the first measured set. The information on the merged data set (with no reflections missing on the main axis) is summarized in Table 1. The first measured data set (TILT_1) contained 7063 reflections (2376 independent ones, 80% completeness, $R_{\rm Wilson}$ = 8.8, $B_{\rm over}$ = 3.3 Å^2) but, owing to the particular orientation of the tilt axis, h00 and 0k0 reflections were missing. The presence of ill-shaped peaks in the Fourier map caused by the absence of these reflections is surely the reason for the difficulties encountered.

The δ recycling method was attempted for the structure solution of charoite90 on the basis of both TILT_1 and merged data sets. Owing to the large number of atoms in the asymmetric unit, phase refinement by δ recycling required us to increase the number of cycles to 1000 to ensure convergence. Using the merged data set, the first $\delta_{\rm P}$ trial (5 min per trial) already gave the complete structure whereas for $\delta_{\rm M}$ three trials were necessary. The respective residuals for the correct solutions are $R_{\rm CC}$ = 17.3 (92 peaks) and $R_{\rm CC}$ = 17.9 (92 peaks).

To investigate if the crystal structure could be solved in a limited number of trials when only TILT_1 data are considered, 100 $\delta_{\rm P}$ trials were calculated (5 min per trial). Two of them converged to the correct solutions: $R_{\rm CC}$ = 32–44 (102 peaks); Corr = 0.874–0.870. For wrong solutions: $R_{\rm CC}$ = 51–76; Corr = 0.864–0.852. The resulting Fourier map corresponding to the complete structure is shown in Fig. 4.

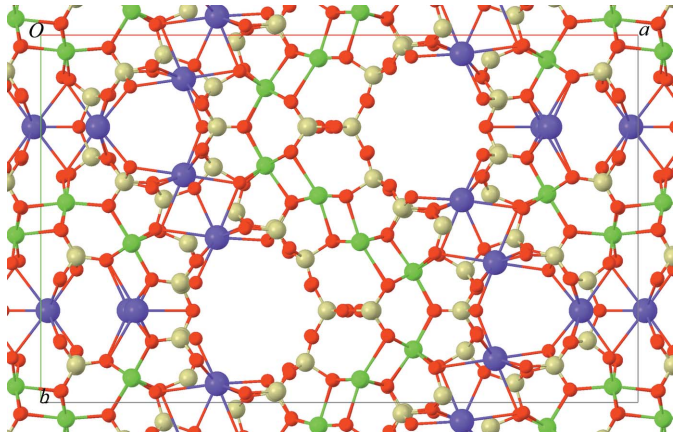

Figure 4
Charoite90: Fourier peaks after $\delta_{\rm P}$ recycling from TILT_1 data (default atom-type assignment based on scattering powers has been revised). Large circles (blue): K; medium circles (green): Ca, Na; medium circles (yellow): Si; small circles (red) O atoms.

Since CHA90 has 20 symmetry-independent Si tetrahedra in the unit cell, the geometrical improvement introduced by merging two data sets can be quantified by analysing the Si—O bond lengths. In the case of the TILT_1 data set, the average value of all individual tetrahedral mean bond lengths is 1.64 (4) Å. Similarly, the average value of the corresponding individual standard deviations is 0.09 (4) Å. For the merged data set, the respective values are 1.63 (4) and 0.06 (3) Å, *i.e.* whereas the average value of the mean bond lengths is practically the same, the average value of the standard deviations is much lower for merged data. This result is to be expected, since the introduction of the second set helps to better define the peaks in the Fourier synthesis, so that the peak centres can be fixed more accurately.

4.4. ITQ-43: δ recycling in the presence of the organic template

ITQ-43 is a large-pore germano-silicate zeolite synthesized with the (2′*R*,6′*S*)-2′,6′-dimethylspiro[isoindoline-2,1′-piperidin]-1′-ium molecule as the structure-directing agent. Although the presence of the template and the consequent diffuse scattering affected the quality of the ADT data, the framework model could be determined by conventional direct methods in space group *C*222 with a residual $R(F)$ of 33.8% and with almost half of the oxygen positions missing (Mugnaioli & Kolb, 2013). The final structure model was refined in *Cmmm* against the PXRD data of a calcinated sample collected in a controlled atmosphere (Jiang *et al.*, 2011). The results of the Rietveld refinement mostly confirmed the positions of the Si atoms found by electron diffraction with important deviations only for the atoms at the corner of the clover-like mesoporous channel.

To check δ recycling and to complement previous results, phase refinements with $\delta_{\rm M}$ were first carried out in space group *Cmmm* (without considering the template molecules). Forty trials (70 cycles per trial; 2 min per trial) were computed from

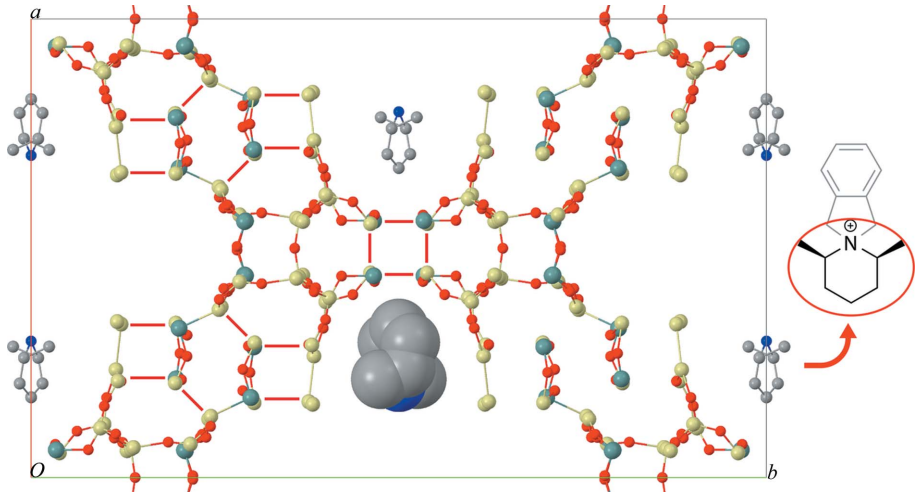

Figure 5
ITQ-43: result of δ_M recycling in *C*222 showing all *T* atoms and most O atoms. To help with recognizing the framework, missing O atoms have been replaced by lines between *T* atoms in the left part of the picture. The template fragment found in the Fourier map is encircled [for clarity, one such fragment (centre-bottom) is in space-filling style].

which four solutions developed the framework atoms. The R_{CC} values are large for both correct and wrong solutions, probably due to the missing organic part not included in the R_{CC} calculation. The figures of merit for the successful runs are: R_{CC} = 67–71; Corr = 0.859–0.856; Cendev = 17.2–19.5°. For the wrong solutions: R_{CC} = 70–88; Corr = 0.855–0.846; Cendev = 22.2–30.1°. The combination of low R_{CC} and low Cendev values allowed identification of the correct solution unambiguously. One of these four correct solutions was further developed by δ recycling in space group *C*222. The resulting R_{CC} value dropped to 39 and one fragment of the template molecule close to the double four-membered rings showed up in the Fourier map (Fig. 5). The identification of this fragment is a clear indication of the correctness of *C*222.

To visualize the effect of the template removal on the ITQ-43 framework, ITQ-43 data were δ_M recycled in *Cmmm* and the resulting *T* (= tetrahedrally coordinated) atom positions compared with the published ones derived from Rietveld refinement of the calcined sample. As can be seen in Fig. 6, the effect of template removal is a significant shrinkage of the framework and the consequent widening of the clover-like mesoporous channel.

4.5. IM-5: structure completion of a large zeolite by δ recycling

IM-5 is one of the most complicated zeolite frameworks ever recognized (24 symmetry-independent Si atoms). It was firstly determined by Baerlocher *et al.* (2007) combining electron diffraction, high-resolution transmission electron microscopy (HRTEM) and PXRD data. Despite the big effort spent on this structure determination, the presence of the inversion centre was not fully demonstrated. The structure was solved again using HRTEM alone, but the question about the inversion centre was kept open (Sun *et al.*, 2010). Recently, a promising ADT data set with an R_{sym} of 16.3% and completeness of 94% down to d_{min} = 1.2 Å was collected on a platelet. Nevertheless, the solution obtained by conventional direct methods on the basis of these data was largely incomplete and only subsequent refinement by Fourier mapping allowed completion of the framework (Mugnaioli & Kolb, 2013).

Calculation of 25 trials of δ_M and δ_P recycling to the same data set already solved the structure in any of the three space groups *C*2*cm*, *Cmc*21 and *Cmcm* (95 cycles per trial; 1.5 min per trial). For the solution in the centrosymmetric *Cmcm* space group, the trial with the smallest R_{CC} value developed the whole structure (bridging O atoms included) thus being a strong indication that it is the true space group. The figures of merit for the successful run are: R_{CC} = 86; Corr = 0.817. For the wrong solutions: R_{CC} = 93–141; Corr = 0.817–0.809. Fig. 7

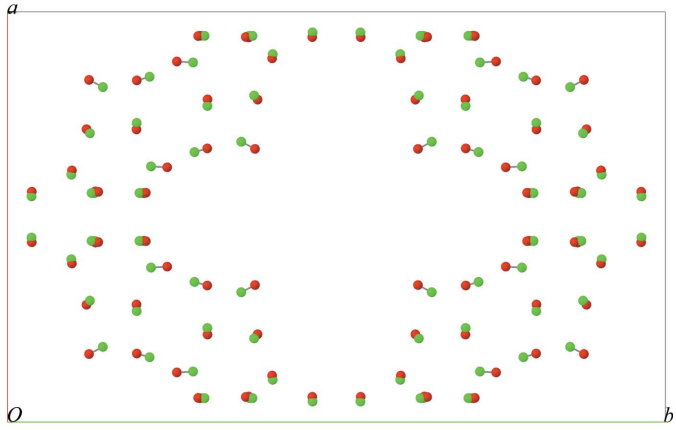

Figure 6
ITQ-43: comparison of the *T*-atom positions for the 'as synthesized' (dark/red circles) and calcined (light/green circles) forms clearly showing the direction and the amount of the framework shrinkage when removing the template molecules. The maximum shrinkage is observed close to the channel centre (1.0 Å) and the minimum at the double four-membered rings (0.3 Å).

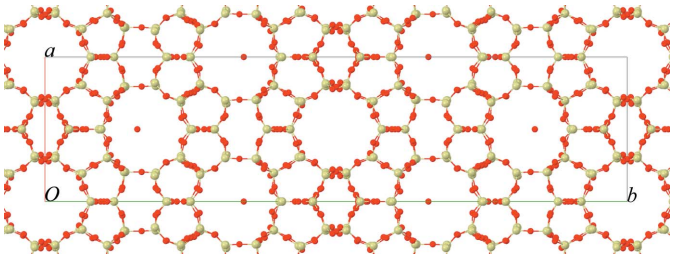

Figure 7
Fourier map (with revised atom-type assignment) resulting from the application of δ_M recycling to ADT data of the IM-5 zeolite. The space group is the centrosymmetric *Cmcm*. Only two O atoms of the framework do not show up in the Fourier map (perspective view of the unit cell along **c**).

shows a perspective view along **c** of the IM-5 structure model after δ_M recycling.

It is noteworthy that, in spite of the high R_{CC} value, practically all O atoms appear close to the expected positions in the Fourier map [average Si—O distance is 1.62 (16) Å]. In this case, since the compound was calcinated, the high R_{CC} value cannot be attributed to the omission of the template in the structure-factor calculation. On the other hand, the fact that almost the complete structure model shows up means that the refined phase values must be far more accurate than reflected by the R_{CC} value. The intensity data of IM-5 were measured on a platelet, so that sample thickening occurs at high tilt angles. The associated large α variability could be an explanation for the high R_{CC} values.

4.6. Aerinite: restrained Rietveld *versus* unrestrained ADT refinements

Aerinite is a fibrous blue silicate mineral that was used as a pigment in many Catalan Romanesque paintings. The studied sample comes from Estopanyà (Huesca, Spain). The major constituents of aerinite are Si, Al, Ca and Fe, and the blue colour is due to the presence of mixed-valence iron (Rius *et al.*, 2004). The approximate composition derived from the present study is given in Table 1. The crystal structure of aerinite was solved from synchrotron powder diffraction data by direct methods followed by restrained Rietveld refinement (Rius, 1993). Although most relevant details of the crystal structure are already known from the powder diffraction study, there are still some intriguing aspects, *e.g.* the exact positions of the metal sites along the columns of face-sharing octahedra which could not be investigated in detail due to the complexity of the crystal structure and to the need to introduce distance restraints when using powder data. To clarify this point, ADT data were collected. Advantage was taken of the large number of symmetry-equivalent reflections in *P*3*c*1 (in most cases with redundancies between 6 and 8 for the collected data) to check the internal accuracy of the ADT intensities. In Fig. 8 the standard deviation σ_I of each group of symmetry-related intensities is plotted as a function of the corresponding average intensity I (reflections with less than four measured symmetry-equivalent reflections were omitted; d_{min} = 0.70 Å).

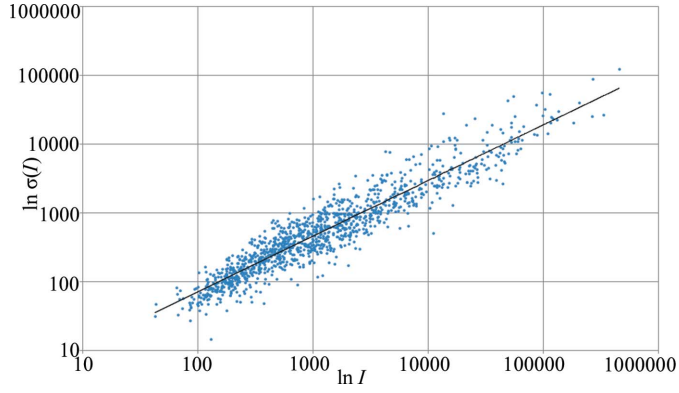

Figure 8
Aerinite: standard deviations of the intensities of symmetry-equivalent reflections plotted *versus* corresponding average intensity values. The equation of the fitted line is $\ln(\sigma_I) = \ln(1.732) + 0.81 \ln(I)$ with $r^2 = 0.8858$. No pronounced outliers are detected.

It can be seen that the fractional standard deviations of the intensities follow the general trend, $\sigma_I / I \propto 1/I^{0.19}$, *i.e.* they are somewhat larger than expected for only counting statistics errors, $1/I^{1/2}$.

From the 25 δ_P trials of random starting phases, 24 trials yielded the correct solution in 100 cycles (5 s per trial). The figures of merit for correct solutions are: R_{CC} = 21–25; Corr = 0.881–0.861; Cendev = 7–11°. As already established in preceding studies (Rius *et al.*, 2004, 2009), the metal sites (*A* and *B*) in the two symmetry-independent columns of face-sharing octahedra are predominantly occupied by Fe and Al atoms (Fig. 9).

The scattering powers were refined with *SHELX97* (Sheldrick, 2008) and correspond to the composition 0.984 (42) Fe

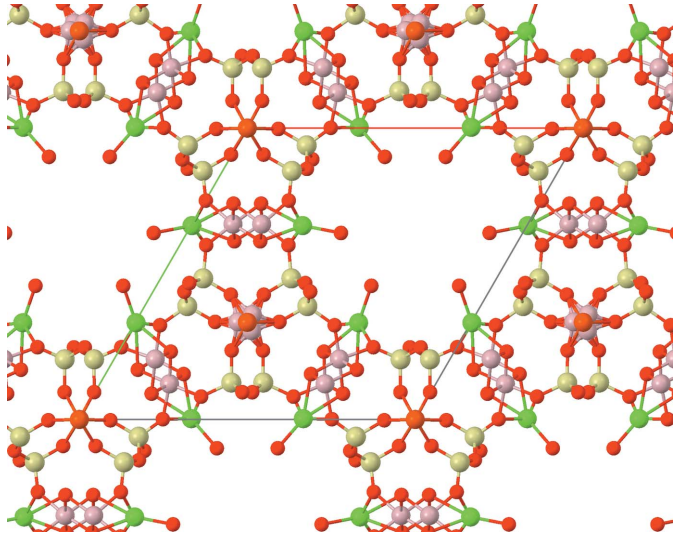

Figure 9
Aerinite: perspective view of the crystal structure along **c**. The three basic structural units can be clearly distinguished: the two symmetry-independent columns of face-sharing octahedra at (x, y) = (0, 0) and (2/3, 1/3) and, in between, the brucite-like slab of Al octahedra with the Ca sites paving the channel walls. Metal sites *A* and *B* are at the centres of the octahedra at (0, 0) and (2/3, 1/3), respectively.

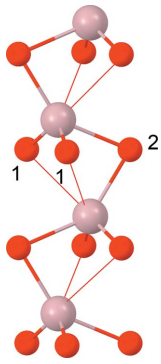

Figure 10
Aerinite: distribution of the highly distorted B_{Al} site along the column of face-sharing octahedra at (x = 2/3, y = 1/3). For a given B_{Al} position the refined distances to the six corners of the octahedron are 1.64 (3), 1.68 (3), 2.13 (4), 2.24 (4), 2.59 (4) and 2.60 (4) Å. The only possible arrangement explaining this result is the formation of Al domains where the O ligands labelled with 1 in the figure are bound to one Al (bond strength ∼1 v.u.) and to one Si of the pyroxene-type chain (not reproduced), whereas those denoted by 2 are linked to two Al atoms (ideally 0.5 v.u. each one) and one Si. This arrangement produces the largest separation, 2.77 (2) Å, between consecutive Al atoms and confers to each Al atom a distorted tetrahedral coordination (the two longest Al···O distances plotted as thin lines are considered as too weak interactions). According to the existence of the ternary symmetry axis in $P3c1$, each B_{Al} site is averaged at three positions.

for site A and 0.677 (50) Fe + 0.323 (50) Al for site B, *i.e.* ideally 1, 2/3 and 1/3. Because of the unequal Fe—O and Al—O bond distances the B site was split in two (B_{Fe} and B_{Al}) and in the last refinement anisotropic U's were introduced for all atoms (except for the B_{Al} site, for which the isotropic U was retained). Because of the large number of independent reflections (2600 reflections for 129 parameters; d_{min} = 0.70 Å) no restraints were required. Final figures of merit are $R1$ = 0.2133 for 2302 $F_o > 4\sigma(F_o)$; $R1$ = 0.2285, $wR2$ = 0.5248 and GoF = 3.15 for all data. Average bond distances (given in Å) of the two symmetry-independent Si tetrahedra and of the Al octahedra of the brucite-like slab are: SiA—O: 1.61 (6) (4×); SiB—O: 1.64 (4) (4×); Al—O: 1.91 (7) (6×). For site A, the average Fe—O distance is 2.035 (9) Å (2×), which indicates that it is mostly Fe^{3+} (average Fe^{3+}—O and Fe^{2+}—O distances are 2.015 and 2.14 Å, respectively). For site B_{Fe}, the refined average Fe—O distance is 2.078 (9) Å (2×), *i.e.* just halfway between the Fe^{3+}— and Fe^{2+}—O distances, which confirms the presence of mixed-valence $Fe^{2.5+}$ (Rius *et al.*, 2009). For site B_{Al}, the fact that the refined atomic displacement parameters of the apical O atoms of the Si tetrahedra take normal values for the principal mean-square atomic displacement U's (0.054, 0.035 and 0.032 Å^2) combined with the much shorter Al—O distance compared to the $Fe^{2.5+}$—O one (respective theoretical distances are 1.91 and approximately 2.08 Å) forces the B_{Al} site to be highly distorted (and disordered). The distribution of the B_{Al} site is described in detail in Fig. 10. According to these results the respective compositions for the A and B columns of face-sharing octahedra are $[Fe_2^{3+}O_6]^{6-}$ and $[(Fe_{1.33}^{2.5+}Al_{0.67})O_6]^{6.67-}$. This example clearly shows the feasibility of performing detailed structural analyses from ADT data when assisted with complementary information. Particularly favourable (in comparison to powder diffraction) is the large number of observed intensities that relaxes the need for restraints in the refinement, thus reducing the possibility of obtaining biased results.

5. Conclusions

Up to now, crystal structure determination of inorganic compounds from ADT data has mostly been performed by conventional direct methods and charge flipping as implemented in *SIR2011* (Burla *et al.*, 2012) and in *Superflip* (Palatinus & Chapuis, 2007), respectively. Even if the results are generally good, these protocols show their limits for complex inorganic structures, such as large-pore zeolites (Mugnaioli & Kolb, 2013). The main problem is the deviation between experimentally measured and theoretical kinematical structure factors, which is still a major problem for the phasing of structures with large cell parameters by direct methods. The combination of δ recycling with ADT discussed in the present study allows us to conclude that this procedure, which makes full use of the atomicity and of the knowledge of the approximate unit-cell contents during the phasing process, represents a fast and robust alternative to already existing methods. For some complex zeolites like IM-5 the results obtained by δ recycling are definitely clearer than those obtained by conventional direct methods. Also particularly interesting is the observation that the Wilson-plot scaling procedure is largely insensitive to gauging volume variations during data collection.

At present, the application of δ recycling is restricted to inorganic compounds. For hybrid and organic materials, the low resolution of the diffraction patterns as well as the unavoidable deterioration of the sample during data acquisition produce ADT data of poorer quality, which makes the application of δ recycling difficult.

JR acknowledges the financial support of the Ministerio de Economia y Competividad (Projects MAT2009-07967, MAT2012-35247, Consolider NANOSELECT CSD2007-00041) and the Generalitat de Catalunya (SGR2009). OV also thanks NANOSELECT for a contract. EM and UK thank SFB 625 and Stiftung Rheinland Pfalz für Innovation. The aerinite sample was kindly provided by Professor Ignaci Queralt from 'Institut Jaume Almera' (CSIC) and the aerinite ADT data were collected by Dr Tatiana Gorelik (University of Mainz).

References

Baerlocher, C., Gramm, F., Massüger, L., McCusker, L. B., He, Z., Hovmöller, S. & Zou, X. (2007). *Science*, **315**, 1113–1116.
Birkel, C. S., Mugnaioli, E., Gorelik, T., Kolb, U., Panthöfer, M. & Tremel, W. (2010). *J. Am. Chem. Soc.* **132**, 9881–9889.
Brese, N. E. & O'Keeffe, M. (1991). *Acta Cryst.* B**47**, 192–197.
Burla, M. C., Caliandro, R., Camalli, M., Carrozzini, B., Cascarano, G. L., Giacovazzo, C., Mallamo, M., Mazzone, A., Polidori, G. & Spagna, R. (2012). *J. Appl. Cryst.* **45**, 357–361.

Cowley, J. M. (1992). *Electron Diffraction Techniques*, Vol. 1. Oxford University Press.
Denysenko, D., Grzywa, M., Tonigold, M., Streppel, B., Krkljus, I., Hirscher, M., Mugnaioli, E., Kolb, U., Hanss, J. & Volkmer, D. (2011). *Chem. Eur. J.* **17**, 1837–1848.
Doyle, P. A. & Turner, P. S. (1968). *Acta Cryst.* A**24**, 390–397.
Dudka, A. P., Avilov, A. S. & Nicolopoulos, S. (2007). *Ultramicroscopy*, **107**, 474–482.
Feyand, M., Mugnaioli, E., Vermoortele, F., Bueken, B., Dieterich, J. M., Reimer, T., Kolb, U., de Vos, D. & Stock, N. (2012). *Angew. Chem. Int. Ed.* **124**, 10519–10522.
Gemmi, M., Campostrini, I., Demartin, F., Gorelik, T. E. & Gramaccioli, C. M. (2012). *Acta Cryst.* B**68**, 15–23.
Gemmi, M. & Oleynikov, P. (2013). *Z. Kristallogr.* **228**, 51–58.
Gorelik, T. E., Stewart, A. A. & Kolb, U. (2011). *J. Microsc.* **244**, 325–331.
Gorelik, T. E., van de Streek, J., Kilbinger, A. F. M., Brunklaus, G. & Kolb, U. (2012). *Acta Cryst.* B**68**, 171–181.
Jansen, J., Tang, D., Zandbergen, H. W. & Schenk, H. (1998). *Acta Cryst.* A**54**, 91–101.
Jiang, J., Jorda, J. L., Yu, J., Baumes, L. A., Mugnaioli, E., Diaz-Cabanas, M. J., Kolb, U. & Corma, A. (2011). *Science*, **333**, 1131–1134.
Kokotailo, G. T., Lawton, S. L., Olson, D. H. & Meier, W. M. (1978). *Nature (London)*, **272**, 437–438.
Kolb, U., Gorelik, T., Kübel, C., Otten, M. T. & Hubert, D. (2007). *Ultramicroscopy*, **107**, 507–513.
Kolb, U., Gorelik, T. E., Mugnaioli, E. & Stewart, A. (2010). *Polym. Rev.* **50**, 385–409.
Kolb, U., Gorelik, T. & Otten, M. T. (2008). *Ultramicroscopy*, **108**, 763–772.
Kolb, U., Mugnaioli, E. & Gorelik, T. E. (2011). *Cryst. Res. Technol.* **46**, 542–554.
Main, P. (1979). *Acta Cryst.* A**35**, 779–785.
Mentzen, B. F. (2007). *J. Phys. Chem.* **111**, 18932–18941.
Mott, N. F. & Massey, H. S. W. (1965). *The Theory of Atomic Collisions.* Oxford: Clarendon.
Mugnaioli, E., Gorelik, T. & Kolb, U. (2009). *Ultramicroscopy*, **109**, 758–765.
Mugnaioli, E. & Kolb, U. (2013). *Micropor. Mesopor. Mater.* **166**, 93–101.
Mugnaioli, E., Sedlmaier, S. J., Oeckler, O., Kolb, U. & Schnick, W. (2012). *Eur. J. Inorg. Chem.* pp. 121–125.
Olson, D. H., Kokotailo, G. T., Lawton, S. L. & Meier, W. M. (1981). *J. Phys. Chem.* **85**, 2238–2243.
Palatinus, L. & Chapuis, G. (2007). *J. Appl. Cryst.* **40**, 786–790.
Palatinus, L., Jacob, D., Cuvillier, P., Klementová, M., Sinkler, W. & Marks, L. D. (2013). *Acta Cryst.* A**69**, 171–188.
Palatinus, L., Klementová, M., Dřínek, V., Jarošová, M. & Petříček, V. (2011). *Inorg. Chem.* **50**, 3743–3751.
Rius, J. (1993). *Acta Cryst.* A**49**, 406–409.
Rius, J. (2012*a*). *Acta Cryst.* A**68**, 77–81.
Rius, J. (2012*b*). *Acta Cryst.* A**68**, 399–400.
Rius, J., Crespi, A., Roig, A. & Melgarejo, J. C. (2009). *Eur. J. Mineral.* **21**, 233–240.
Rius, J., Elkaim, E. & Torrelles, X. (2004). *Eur. J. Mineral.* **16**, 127–134.
Rozhdestvenskaya, I., Mugnaioli, E., Czank, M., Depmeier, W., Kolb, U., Reinholdt, A. & Weirich, T. (2010). *Mineral. Mag.* **74**, 159–177.
Sedlmaier, S. J., Mugnaioli, E., Oeckler, O., Kolb, U. & Schnick, W. (2011). *Chem. Eur. J.* **17**, 11258–11265.
Sheldrick, G. M. (2008). *Acta Cryst.* A**64**, 112–122.
Sun, J., He, Z., Hovmöller, S., Zou, X., Gramm, F., Baerlocher, C. & McCusker, L. B. (2010). *Z. Kristallogr.* **225**, 77–85.
Vainshtein, B. K. (1991). *Acta Cryst.* B**47**, 145–154.
Vincent, R. & Midgley, P. (1994). *Ultramicroscopy*, **53**, 271–282.
Wilson, A. J. C. (1942). *Nature (London)*, **150**, 152.
Zhang, D., Oleynikov, P., Hovmöller, S. & Zou, X. (2010). *Z. Kristallogr.* **225**, 94–102.